ADVANCES IN ATMOSPHERIC SCIENCES, VOL. 38, JULY 2021, 1252–1263

• **Original Paper** •

Photooxidation of Methacrolein in Fe(III)-Oxalate Aqueous System and Its Atmospheric Implication

Yu WANG[1], Jie ZHAO[1], Huihui LIU[1], Yuan LI[1], Wenbo DONG[*1,2], and Yanlin WU[1,2]

[1]*Shanghai Key Laboratory of Atmospheric Particle Pollution and Prevention*, *Department of Environmental Science & Engineering*, *Fudan University*, *Shanghai* 200438, *China*

[2]*Shanghai Institute of Pollution Control And Ecological Security*, *Shanghai* 200092, *China*

(Received 16 December 2020; revised 19 April 2021; accepted 10 May 2021)

ABSTRACT

Iron and oxalic acids are widely distributed in the atmosphere and easily form ferric oxalate complex (Fe(III)-Ox). The tropospheric aqueous-phase could provide a medium to enable the photo-Fenton reaction with Fe(III)-Ox under solar irradiation. Although the photolysis mechanisms of Fe(III)-Ox have been investigated extensively, information about the oxidation of volatile organic compounds (VOC), specifically the potential for Secondary Organic Aerosol (SOA) formation in the Fe(III)-Ox system, is lacking. In this study, a ubiquitous VOC methacrolein (MACR) is chosen as a model VOC, and the oxidation of MACR with Fe(III)-Ox is investigated under typical atmospheric water conditions. The effects of oxalate concentration, Fe(III) concentration, MACR concentration, and pH on the oxidation of MACR are studied in detail. Results show that the oxidation rate of MACR greatly accelerates in the presence of oxalate when compared with only Fe(III). The oxidation rate of MACR also accelerates with increasing concentration of oxalate. The effect of Fe(III) is found to be more complicated. The oxidation rate of MACR first increases and then decreases with increasing Fe(III) concentration. The oxidation rate of MACR increases monotonically with decreasing pH in the common atmospheric water pH range or with decreasing MACR concentration. The production of ferrous and hydrogen peroxide, pH, and aqueous absorbance are monitored throughout the reaction process. The quenching experiments verify that $^{\cdot}OH$ and O_2^- are both responsible for the oxidation of MACR. MACR is found to rapidly oxidize into small organic acids with higher boiling points and oligomers with higher molecular weight, which contributes to the yield of SOA. These results suggest that Fe(III)-Ox plays an important role in atmospheric oxidation.

Key words: Fe(III)-Ox, OH radical, atmospheric oxidation, SOA, methacrolein

Citation: Wang, Y., J. Zhao, H. H. Liu, Y. Li, W. B. Dong, and Y. L.Wu, 2021: Photooxidation of methacrolein in Fe(III)-Oxalate aqueous system and its atmospheric implication. *Adv. Atmos. Sci.*, **38**(7), 1252−1263, https://doi.org/10.1007/s00376-021-0415-5.

Article Highlights:

- The oxidation mechanism of methacrolein is investigated in the Fe(III)-Ox system in atmospheric water, indicating that O_2^- can directly oxidize MACR.
- The Fe(III)-Ox Fenton-like reaction in the atmosphere increases the absorbance of aerosols and has implications for radiative forcing.
- Methacrolein is rapidly oxidized into small organic acids with higher boiling points and oligomers with higher molecular weight in the Fe(III)-Ox Fenton-like system, which contributes to the yield of SOA.

1. Introduction

Tropospheric aqueous-phase chemistry plays a key role in the formation of oxidizing species in the atmosphere (Hermann et al., 2015). Iron is the most abundant transition metal element in tropospheric particles. It enters the atmosphere through various ways, such as sea spray (Guasco et al., 2014), combustion and industrial activities, and from the earth via wind (Liati et al., 2013; Li et al., 2016). Fenton reaction caused by the presence of iron is widespread in the atmosphere (Deguillaume et al., 2004). Some studies (Nguyen et al., 2013; Chu et al., 2014) have indicated that the Fenton reaction in the atmosphere mainly happens in the aqueous phase. Some estimates suggest that Fenton reaction involving iron might account for ~30% of the $^{\cdot}OH$ produc-

* Corresponding author: Wenbo DONG
Email: wbdong@fudan.edu.cn

tion in fog droplets (Deguillaume et al., 2005). The oxidizing ability contributed from Fenton reaction is highly dependent on pH, iron concentration, and the kind and concentration of organic compounds that form complexes with iron (Zuo and Hoigne, 1992; Weller et al., 2013b, a). Notably, the formation of iron complexes have a significant effect on the photochemical reaction pathway. Iron can complex with oxalic acid, which was the most abundant dicarboxylic acid in aqueous aerosol (Sorooshian et al., 2006; Legrand et al., 2007), and the ferric oxalate complex (Fe(III)-Ox) can efficiently produced oxidized species by photo-reduce Fe(II) under relevant atmospheric condition (Thomas et al., 2016). Oxalic acid is an ultimate end product in the oxidation of organic compounds in atmosphere such as isoprene and aromatic hydrocarbons (Boreddy et al., 2017). Oxalic acid could also come from incomplete combustion. One simulation has shown that at least 50% of Fe(III) is bound by oxalic acid during both cloud and deliquescent particle periods because of their strong complexing coefficients (Weller et al., 2014), and 99% of oxalic acid is consumed by photolysis. Field observations have also shown a significant negative correlation between atmospheric oxalic and Fe(III) concentrations (Sorooshian et al., 2013). Photolysis of Fe(III)-Ox in the atmosphere is extensive. Thus, it is necessary to evaluate its effect on atmospheric oxidation. Although the photochemistry of Fe(III)-Ox has been studied extensively, knowledge of its impact on the aging of atmospheric organic matter, especially a volatile organic compound (VOC) with a low boiling point in the aqueous phase, is still inadequate (Thomas et al., 2016; Pang et al., 2019). There is a potential for secondary aerosol formation when a VOC with a low boiling point transfers to a product with a higher boiling point.

Isoprene (2-methyl-1,3-butadiene, C_5H_8) is a widespread biogenic hydrocarbon (Seinfeld and Pandis, 2016) that relates closely to photosynthetic activity in plants. Its main oxidation product is methacrolein (C_4H_6O, MACR), which occupies about 22% of the yield of isoprene. MACR is a model compound in photochemical experiments. Although MACR has a small Henry coefficient ($H_{methacrolein} = 6.5\ M\ atm^{-1}$), its concentration in the aqueous phase is found to be much higher than expected based only on its Henry coefficient (van Pinxteren et al., 2005). Thus, MACR is a typical representative VOC in the aqueous phase. The oxidation mechanism of MACR has been investigated previously in many studies (Zhang et al., 2010; Liu et al., 2012; Schöne et al., 2014; Giorio et al., 2017), allowing for easy comparisons.

This study explores the aqueous photo-Fenton reaction involved in the oxidation of MACR in the presence of Fe(III)-Ox. The effects of oxalate concentration, Fe(III) concentration, MACR concentration, and pH are analyzed. The main long-lived oxidation species, Fe(III) and H_2O_2, in photo-Fenton reaction are measured. The kinds and abilities of free radicals involved in the reaction with MACR are evaluated. The photodegradation mechanism and the possible oxidative products are studied by liquid-chromatography quadrupole time-of-flight mass spectrometry (LC-QTOF-MS). The oxidation products (namely, small organic acids) are analyzed by ion chromatograph (IC). Furthermore, the absorbance of the aqueous solution is tracked by a UV-vis spectrometer. The results obtained in this study will provide a reference for predicting the influence of low boiling-point VOCs in photooxidation with Fe(III)-carboxylic complexes in atmospheric water.

2. Materials and methods

2.1. *Materials*

MACR (95%) and potassium oxalate (99.98%) were purchased from Shanghai Aladdin Bio-Chem Technology Co. Ltd. Ferric perchlorate, perchloric acid (70%), ferrozine (97%), 4-hydroxyphenylacetic acid (99%), and peroxidase (from horseradish, RZ>2.5) were purchased from Sigma-Aldrich. Analytical grade CH_3COOH, CH_3COONa, NaOH, hydroxylamine hydrochloride, phenazine, and ethylenediaminetetraacetic acid disodium salt (EDTA-2Na) were purchased from Sinopharm Chemical Reagent Co., Ltd. Deionized (DI) water was utilized in all experiments.

2.2. *Photolysis experiments*

Photolysis reaction was performed in a photochemical reactor (XPA-VII, Xujiang electromechanical plant, Nanjing, China) equipped with a 500 W Xenon lamp combined with a 290 nm cut-off filter as simulated solar light. The Xenon lamp spectrum received by the reaction solution is shown in Fig. A1 in the Appendix. The temperature of the reactor was maintained at 25°C ± 2°C by cooling water. The pH was adjusted by $HClO_4$. A 20 mL solution was prepared under constant magnetic stirring and reacted in a 50 mL cylindrical quartz tube sealed with a rubber stopper. Before sealing, the aqueous solution, which did not contain MACR, was stirred in the dark for 10 min to achieve oxygen saturation. Then, 1 mL of the solution was taken out through the rubber stopper using a syringe and filtered through a poly tetra fluoroethylene (PTFE) 0.22 μm filter.

2.3. *Analytical procedures*

GC-FID (Agilent 7890A, USA) was used to analyze the MACR concentration. It was equipped with a semi-polar capillary column (CNW CD-5MS 30 m × 0.25 mm × 0.25 μm, Germany), which allowed the injection of aqueous phase samples. The GC injector and detector were heated at 250°C. Nitrogen gas was used as carrier gas at 1 mL min^{-1} with a 1/10 split. The oven temperature program was 40°C for 4 min, raised by 10°C min^{-1} up to 120°C, and 120°C for 5 min (El Haddad et al., 2009; Liu et al., 2009).

An IC (DIONEX ICS-3000, Thermo Fisher, USA) assembled with AG11-HC guard column and AS11-HC analytical column was used to measure organic acid anions (Zhou et al., 2018). The pH of the aqueous solution containing iron ion was adjusted to 10. Then, the solution was

passed through a 0.22 μm PTFE filter and an H-type pretreatment filter to remove the iron.

The concentrations of Fe(II) and total dissolved iron were determined by using a spectrophotometry methodology with ortho-phenanthroline and hydroxylamine (Sastry and Rao, 1996). Hydrogen peroxide concentrations were determined by the fluorescence method developed by Lazrus et al. (1985) after sample mixing with EDTA-2Na. Solution pH was measured using a pH meter (METTLER TOLEDO FE20, Switzerland). UV-vis spectra of the solutions were tracked by UV-vis spectrometer (Scinco Nano MD, SCINCO, South Korea).

Reaction byproducts were identified with a LC-QTOF-MS system (Agilent 6540, USA) equipped with an electrospray ionization source, and analysis was performed under negative ionization mode (Lian et al., 2017).

3. Results and discussion

3.1. *The control experiments*

As seen in Fig. 1, MACR shows little change under dark conditions. The small Henry coefficient of MACR keeps it mostly distributed in the aqueous solution, and errors caused by gas-liquid distribution are ignored in subsequent experiments. No obvious direct photolysis of MACR is found under the simulated sunlight conditions (λ > 290 nm) because MACR's absorbance peak at 375 nm is low (Fig. 2). In the presence of Fe(III), MACR is oxidized about 7% in 90 min. $Fe(OH)^{2+}$ is the dominant Fe(III) hydroxide complex in the aqueous solution with pH of 4, and it is expected to undergo photolysis to generate ·OH according to Eqs. (1–3) and then react with MACR.

$$Fe(III) + H_2O \rightarrow [Fe(III)(OH)]^{2+} + H^+ , \quad (1)$$

$$[Fe(III)(OH)]^{2+} + h\nu \rightarrow Fe(II) + {}^{\cdot}OH , \; k = 0.0012\ s^{-1} \text{(Balmer and Sulzberger, 1999)} , \quad (2)$$

where h is Planck constant, ν is frequency of light.

$$Fe^{2+} + H_2O_2 \rightarrow Fe^{3+} + OH^- + {}^{\cdot}OH . \quad (3)$$

In the presence of Fe(III)-Ox (Fig. 1), the oxidation rate of MACR rapidly increases, and 80% MACR is oxidized in 60 min. This result occurs because Fe(III)-Ox forms and the efficiency of Fenton-like reaction is accelerated. As shown in Fig. A2, Fe(III)-Ox has more obvious absorption peaks in the sunlight range compared to the Fe(III) solution. Quantum yields (at 293 K, pH = 4.0) for the photolysis of $Fe(OH)^{2+}$ at 313 nm and 360 nm are 0.14 ± 0.04 and 0.017 ± 0.003 (Faust and Hoigné, 1990), respectively. $Fe(OH)^{2+}$ has weak absorption in the solar UVA-visible region (Knight and Sylva, 1975). Quantum yields for $[Fe(III)(C_2O_4)_3]^{3-}$ at 313 nm and 366 nm are 2663 ± 37 and 709 ± 10, respectively, and quantum yields for $[Fe(III)(C_2O_4)_2]^-$ at 313 nm and 366 nm are 2055 ± 111 and 1.17 ± 1.46 (Weller et al., 2013b), respectively, which are much higher than $Fe(OH)^{2+}$, indicating that higher photoactivity produces more radicals.

3.2. *Effect of oxalate concentration*

The effect of oxalate concentration is investigated in the range from 100 μM to 2000 μM. As shown in Fig. 2a, the oxidation rate of MACR increases with increasing oxalate concentration. The pseudo-first-order oxidation rate of MACR has an increase of nearly equal proportion with increasing oxalate concentration from 100 μM to 2000 μM (Fig. 2b). Approximately 80% MACR is oxidized when oxalate concentration is 1000 μM. Oxalate at 2000 μM leads to the oxidation of all MACR, though this concentration is excessive. However, the oxidation rate corresponding to 2000 μM oxalate still increases linearly, and the inhibitory effect caused by excess oxalate is not observed in Fig. 2b. This result may be due to the low second-order reaction rate constant of oxalate and ·OH.

The increasing degradation efficiency of MACR is due to the formation of Fe(III)-Ox, which is photolyzed to yield oxalate radicals ($C_2O_4^{\cdot-}$) and ·OH in the presence of dissolved oxygen (Eqs. 4–10).

$$[Fe(III)(C_2O_4)_3]^{3-} + h\nu \rightarrow [Fe(II)(C_2O_4)_2]^{2-} + C_2O_4^{\cdot-} , \; k = 0.04\ s^{-1} \text{ (Balmer and Sulzberger, 1999)} , \quad (4)$$

$$[Fe(III)(C_2O_4)_2]^- + h\nu \rightarrow Fe^{2+} + C_2O_4^{2-} + C_2O_2^{\cdot-} , \quad (5)$$

$$C_2O_4^{\cdot-} \rightarrow CO_2^{\cdot-} + CO_2 , \; k = 2\times10^6\ s^{-1} \text{(Mulazzani et al., 1986)} , \quad (6)$$

$$CO_2^{\cdot-} + O_2 \rightarrow CO_2 + O_2^{\cdot-} , \; k = 6.5\times10^9\ M^{-1}\ s^{-1} \text{(Weller et al., 2013a)} , \quad (7)$$

$$O_2^{\cdot-} + H^+ \leftrightarrow HO_2^{\cdot} , \quad (8)$$

$$Fe(II) + O_2^{\cdot-}/HO_2^{\cdot} + H^+ \rightarrow Fe(III) + H_2O_2 , \; k = 1.0\times10^7/1.2\times10^6\ M^{-1}\ s^{-1} \text{(Rush and Bielski, 1985)} , \quad (9)$$

$$[Fe(II)C_2O_4] + H_2O_2 \rightarrow [Fe(III)C_2O_4]^+ + {}^{\cdot}OH + OH^- \text{ , } k = 3.1 \times 10^4\ M^{-1}\ s^{-1} \text{(Sedlak and Hoigné, 1993)} . \quad (10)$$

Different ratios of oxalate and ferric form different complexes, and quantum yields for $[Fe(C_2O_4)_2]^-$ are larger than $[Fe(C_2O_4)_3]^{3-}$ under simulated sunlight (Weller et al., 2013a), which indicates that $[Fe(C_2O_4)_2]^-$ has stronger photoactivity and can produce more active radicals. According to Fig. A3, the proportion of $[Fe(C_2O_4)_2]^-$ increases first then decreases with increasing oxalate concentration from 100 μM to 2000 μM, while $[Fe(C_2O_4)_3]^{3-}$ increases monotonously and becomes the main complex when the concentration of oxalate is above 500 μM. The different proportions of the complex also cause the difference in the photoactivity of the solution. However, the oxidation rate of MACR keeps increasing monotonically with increasing oxalate concentration, which may be due to the simultaneous existence of multiple complexes, resulting in insignificant differences in photoactivity.

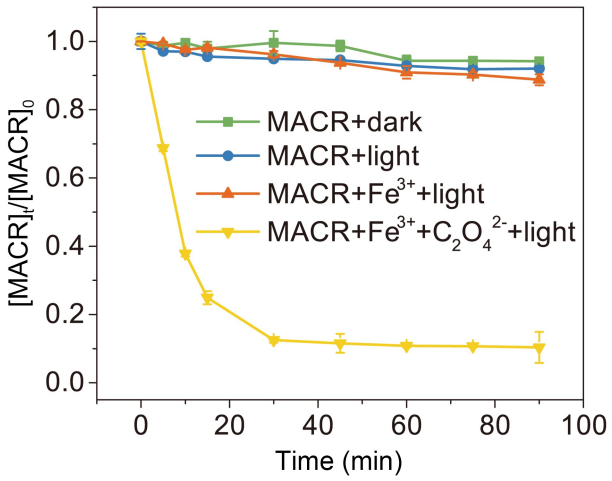

Fig. 1. Control experiments of MACR oxidation ($[MACR]_0$ = 500 μM, $[Fe(III)]_0$ = 100 μM, $[Oxalate]_0$ = 1000 μM, pH = 4.0 ± 0.1, air-saturated solution).

3.3. *Effect of Fe(III) concentration*

To investigate the effect of Fe(III) concentration on the photooxidation of MACR, the Fe(III) concentration was varied from 20 μM to 200 μM during the reaction. As shown in Fig. 3, the photooxidation rate of MACR increases with increasing Fe(III) concentration from 20 μM to 200 μM in the first 60 min. This is because the complex species

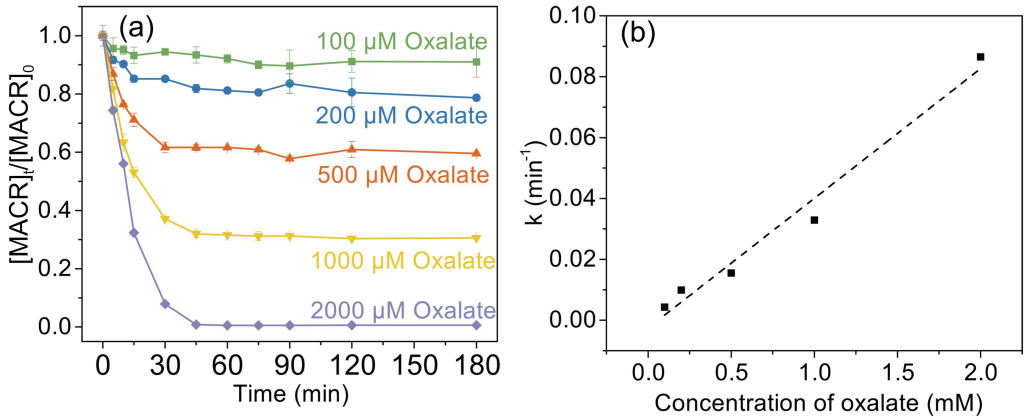

Fig. 2. (a) Effect of oxalate concentration on the photooxidation of MACR in the Fe(III)-Ox system; (b) The reaction rate constant calculated by the pseudo-first-order kinetics variation with the concentration of oxalate ($[Oxalate]_0$ = 1000 μM, $[MACR]_0$ = 500 μM, pH 4.0 ± 0.1, air saturated solution).

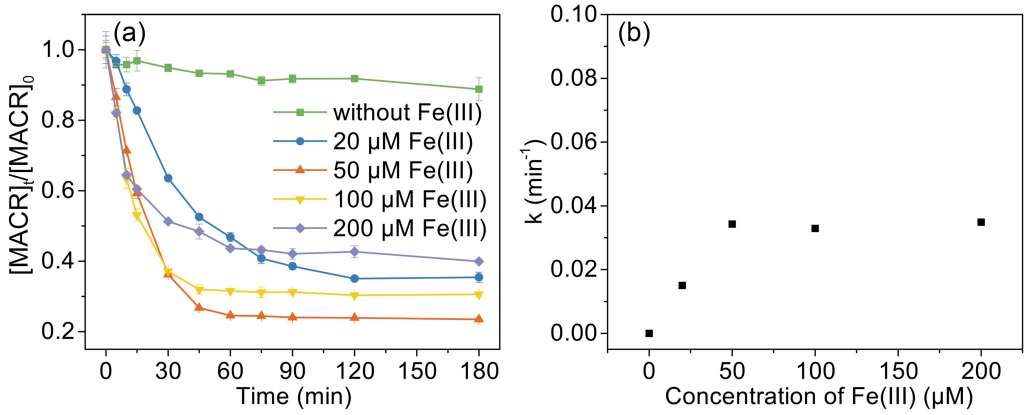

Fig. 3. Effect of Fe(III) concentration on the photooxidation of MACR in the Fe(III)-Ox system ($[Oxalate]_0$ = 1000 μM, $[MACR]_0$ = 500 μM, pH 4.0 ± 0.1, air-saturated solution).

become different when the concentration ratio between ferric and oxalate is changed. The $[Fe(C_2O_4)_2]^-$ with higher photoactivity is the main form when oxalate concentration is low, and more $[Fe(C_2O_4)_3]^{3-}$ is produced with increasing oxalate concentration (Fig. A4). As the reaction time is extended, high Fe(III) concentration has a negative effect on MACR oxidation. The reason for this might be the consumption of CO_2^- under relatively high Fe(III) concentration conditions. Normally, CO_2^- reacts with dissolved O_2 and causes formation of H_2O_2 and ·OH at low Fe(III)-Ox concentration. However, the majority of CO_2^- interacts with Fe(III)-Ox, resulting in the formation of Fe(II) and CO_2 (Eq. 11) with a high concentration of Fe(III)-Ox. The formation of OH radicals is inhibited in this situation.

$$[Fe(III)(C_2O_4)_3]^{3-} + CO_2^- \rightarrow [Fe(II)(C_2O_4)_2]^{2-} + CO_2 + C_2O_4^{2-}. \quad (11)$$

3.4. *Effects of solution pH*

Solution pH has an important effect on the speciation and reactivity of Fe(III)-Ox. The typical pH value in the atmosphere is from 2.5 to 5.5. As shown in Fig. 4, the photooxidation rates of MACR decrease with increasing pH from 2.5 to 5.5. $[Fe(III)(C_2O_4)_2]^-$ is the major complex in pH 2.5 and then decreases with increasing pH value. Then, $[Fe(III)(C_2O_4)_3]^{3-}$ becomes the dominant complex. Considering that $[Fe(III)(C_2O_4)_3]^{3-}$ and $[Fe(III)(C_2O_4)_2]^-$ have stronger photoactivity than $[Fe(III)(C_2O_4)]^+$ and Fe^{3+} (Weller et al., 2013b), pH affects the photo-reactivity by changing the complex forms. Moreover, pH also affects the reactions between O_2^-/HO_2 and Fe(II) (Eq. 9), and these reactions contribute most of the H_2O_2 in the Fe(III) oxalate system. HO_2 is the dominant species at low pH, and then it transfers to O_2^- with increasing pH (Eq. 8) (Zuo and Hoigne, 1992). O_2^- can react to the H_2O_2 form faster than HO_2. So, these two factors allow low pH to have a positive effect on MACR oxidation.

3.5. *Effects of MACR concentration*

The influence of initial MACR concentration (from 60 μM to 680 μM) is investigated (Fig. 5). The oxidation rates of MACR increase with decreasing MACR concentration, and 60 μM, 160 μM, and 250 μM MACR are 100% oxidized during 45 min. However, a certain amount of MACR remains when MACR concentration is high (such as 400 μM and 680 μM). This is because oxalate is depleted and is unable to produce enough ·OH to completely oxidize MACR.

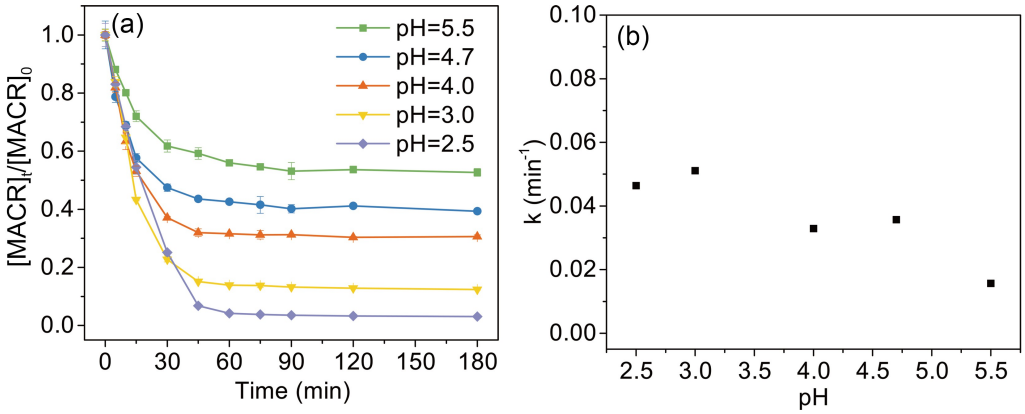

Fig. 4. Effect of pH on the photooxidation of MACR in the Fe(III)-Ox system ($[Fe(III)]_0$ = 100 μM, $[Oxalate]_0$ = 1000 μM, $[MACR]_0$= 500 μM, air-saturated solution).

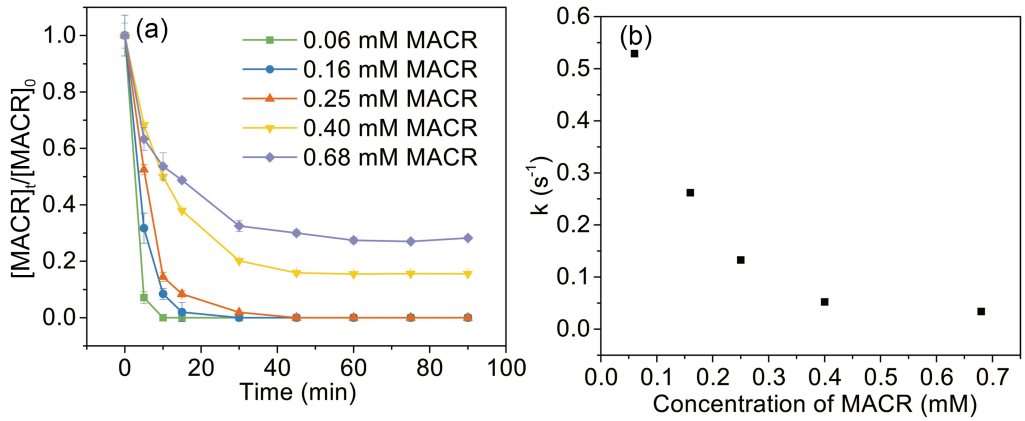

Fig. 5. Effect of MACR concentration on the photooxidation of MACR in the Fe(III)-Ox system ($[Fe(III)]_0$ = 100 μM, $[Oxalate]_0$ = 1000 μM, pH 4.0 ± 0.1, air-saturated solution).

3.6. *Photooxidation mechanism of MACR in Fe(III)-Ox system*

H_2O_2 and Fe(II) are the major long-lived oxidized active species in the photolysis of Fe(III)-Ox (Faust et al., 1993), and this determines the production of free radicals. As shown in Fig. 6a, Fe(II) concentration rapidly increases to 80% in 10 min, and then reduces to approximately 2% from 30 min to 60 min. Finally, Fe(II) concentration is maintained at an undetectable value in the remaining time. The total dissolved iron remains stable for 30 min and then quickly drops to only 5 μM left in the next 30 min. Fe(II) is usually formed by the photoreduction of $[Fe(III)(C_2O_4)_3]^{3-}$ or $[Fe(III)(C_2O_4)_2]^{-}$ and is finally consumed with H_2O_2 to form Fe(III). The accumulation of Fe(II) is due to the fast photoreduction rate. The change of total dissolved iron happens because the iron precipitates as insoluble $Fe(OH)_n(s)$, which is caused by decreasing oxalate concentration (Fig. A3) and increasing pH (Figs. 4. and A5). The change of pH is caused by the generation of OH^- in Fenton reaction. Fenton reaction can increase pH, as confirmed in a previous study (de Lima Perini et al., 2013). The pH increase can be attributed to the consumption of oxalate, leading to the release of Fe(III). The concentration of free oxalate changes, which might establish the acid-base reaction (de Luca et al., 2014). Otherwise, some organic acids are formed by the reaction of MACR and ·OH (Liu et al., 2009), which can decrease the solution pH.

The concentration of H_2O_2 increase in the first 5 min, then decreases in 5–45 min, and returns to increase after 45 minutes (Fig. 6b). H_2O_2 is the production of reaction of Fe(II) and $O_2^{\cdot-}/HO_2^{\cdot}$, and $O_2^{\cdot-}/HO_2^{\cdot}$ is from the photolysis of oxalate (Eqs. 4–9). According to Eqs. 9 and 10, low concentration Fe(II) is suitable for H_2O_2 accumulation, so H_2O_2 concentration increase first and then decrease with the increase of Fe(II) concentration in first 30 min. After 30 min, the increase in pH and the consumption of oxalate leads to the formation of $Fe(OH)_n$, which reduces the available Fe(II) and inhibits the rate of generation and consumption of H_2O_2 (Eqs. 9 and 10) simultaneously. At this stage, non-Fenton reactions might also play a role in the generation and consumption of H_2O_2 (Eqs. 12 and 13).

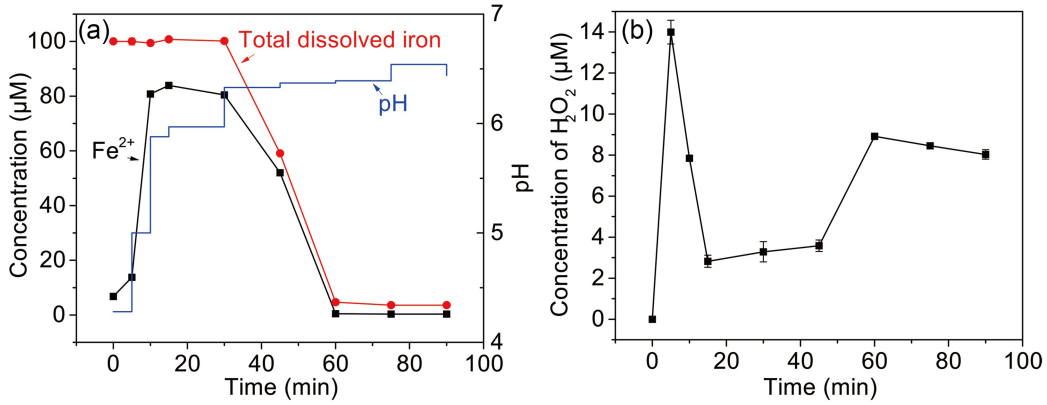

Fig. 6. (a) The change of Fe(II), total dissolved iron, and pH (b) H_2O_2 formation during the photooxidation of MACR in the Fe(III)-Ox system ($[Fe(III)]_0$ = 100 μM, $[Oxalate]_0$ = 1000 μM, $[MACR]_0$ = 500 μM, pH 4.0 ± 0.1, air-saturated solution).

$$HO_2^{\cdot} + O_2^{\cdot-} + H^+ \rightarrow H_2O_2 + O_2\,, \qquad (12)$$

$$H_2O_2 + h\nu \rightarrow H_2O + {}^{\cdot}OH\,. \qquad (13)$$

The mechanism of Fe(III)-Ox photolysis is shown in Eqs. 4–11. $Fe(III)(C_2O_4)_3^{3-}$ and $Fe(III)(C_2O_4)_2^{-}$ are photolyzed to produce $C_2O_4^{\cdot-}$ (Eqs. 4–5), which forms $CO_2^{\cdot-}$ through decarboxylation (Eq. 6). $CO_2^{\cdot-}$ reacts with O_2 to produce $O_2^{\cdot-}$(Eq. 7) and leads to the formation of H_2O_2 (Eq. 9). ·OH can be produced continuously by the reaction between Fe(II) and H_2O_2 (Fenton reaction). In this study, 1 mM p-benzoquinone (BQ) was used as the scavenger of $O_2^{\cdot-}$ (Patel and Willson, 1973), and 200 mM isopropanol (2-Pr) was used to quench ·OH. The experimental results are shown in Fig. 7. The addition of BQ and 2-Pr suppresses the oxidation of MACR, and only 10% and 30% oxidation remains after 90 min reaction, respectively. This indicates that $O_2^{\cdot-}$ can also react with MACR in addition to ·OH. Nitrogen (N_2) is introduced in the solution to eliminate oxygen (O_2). However, it

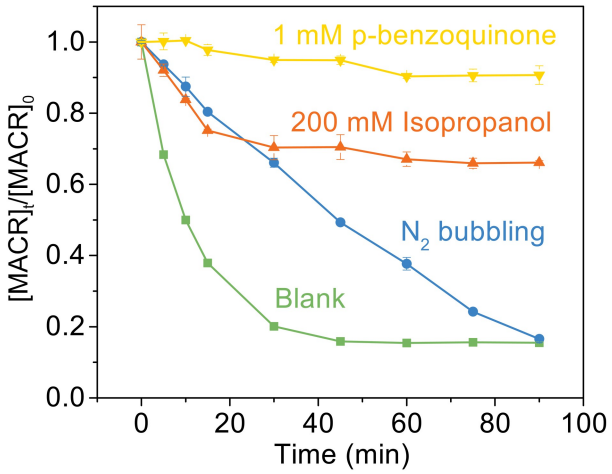

Fig. 7. Effect of scavengers on the photooxidation of MACR in the Fe(III)-Ox system ($[Fe(III)]_0$ = 100 μM, $[Oxalate]_0$ = 1000 μM, $[MACR]_0$ = 500 μM, pH 4.0 ± 0.1, air-saturated solution).

is difficult for the solution containing volatile MACR to remove all O_2 if MACR is prevented from leaking simultaneously. So, the system still contains a part of O_2. However, the N_2 bubbling experiment proves that the conversion of O_2 to O_2^- is an important speed-limiting step. A low concentration of O_2 extends the time for the complete oxidation of MACR. The reaction of MACR with CO_2^- is not considered in aerated water because of the rapid quenching reaction of CO_2^- by O_2 (Surdhar et al., 1989).

The proposed reaction pathways based on the observed products are shown in Fig. 8. Here, we present and discuss the three possible pathways oxidation of MACR in Fe(III)-Ox Fenton-like reaction can proceed: via addition on the C = C bond by ·OH (pathway A) (Liu et al., 2009; Zhang et al., 2010), H-abstraction of the methyl group by ·OH and O_2^- (pathway B), nucleophilic addition on carbonyl group by O_2^- (pathway C) (Hayyan et al., 2016).

The external addition of ·OH leads to the formation of an alkyl radical, which may form aldehyde or react with itself to form polymer $C_8H_{14}O_4$ (Mass-to-charge ratio m/z = 175.0940) directly (pathway A1) or rapidly add to O_2 to form peroxy radical (pathway A2). The peroxy radical reacts with itself to form an unstable tetroxide, then degrades to form alkoxy radical (pathway A2.1). This alkoxy radical undergoes decomposition and forms $C_3H_4O_2$ (m/z = 73.0295), $C_3H_4O_3$ (m/z = 89.0241), $C_3H_6O_2$, and acetic acid (pathway A2.1a, b, c, d). The radical fragments generated during the decomposition can also react with O_2

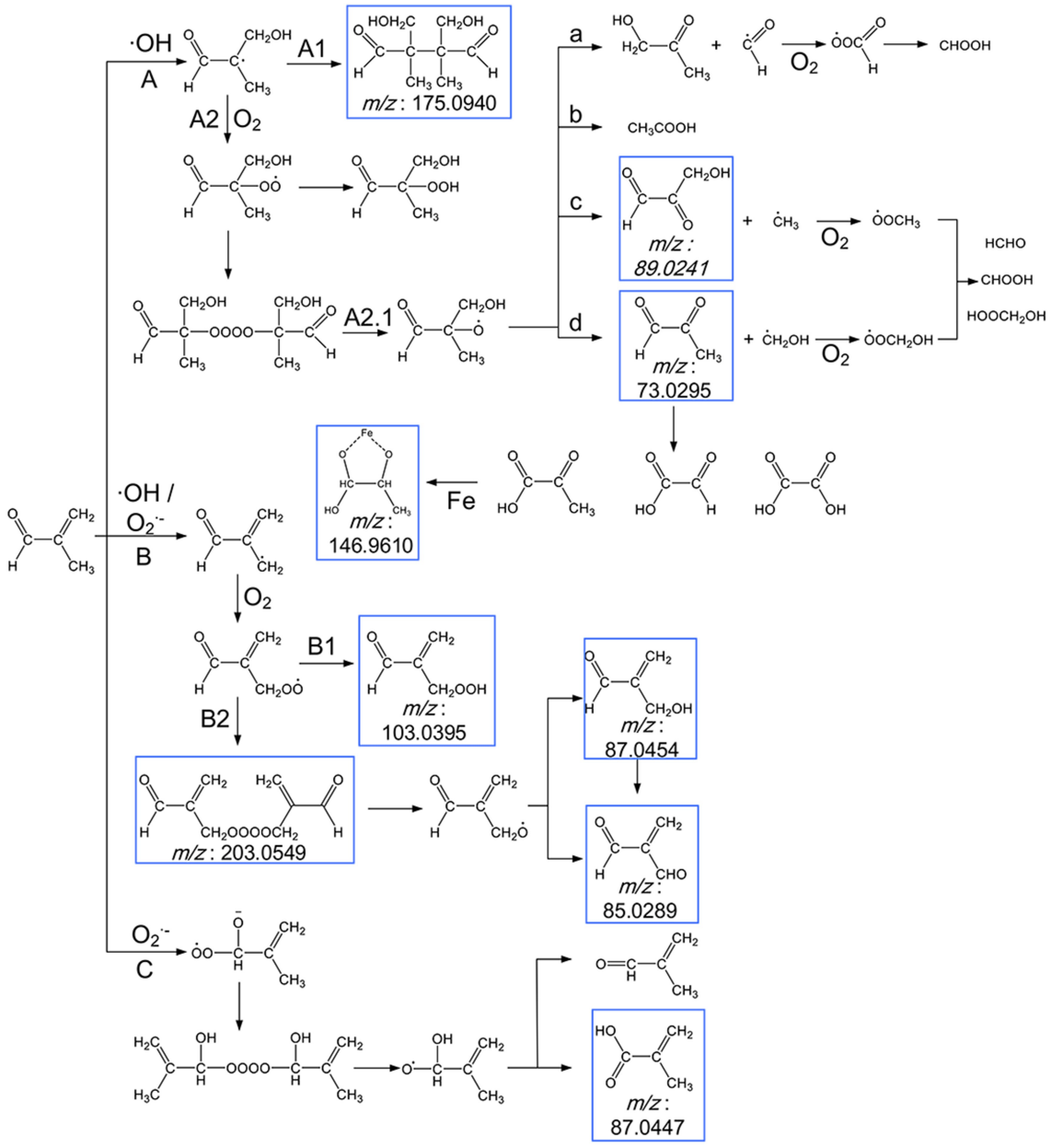

Fig. 8. Scheme for the proposed reaction pathways of the photooxidation of MACR in the Fe(III)-Ox system. The molecular formulas in the blue frames are observed products.

to form HCHO, CHOOH, and $HOOCH_2OH$. The $C_3H_4O_2$ (m/z = 73.0296) can also result in the formation of pyruvate, glyoxylate, and oxalate. $^{\cdot}OH$ and $O_2^{\cdot-}$ can attack MACR by hydrogen abstraction on the methyl group, leading to the formation of the alkyl radical (pathway B). Then by rapidly adding to O_2 to form peroxy radical, which may form the corresponding carboxylic acid $C_4H_6O_3$ (m/z = 103.0395) or react with itself to form a tetroxide $C_8H_{10}O_6$ (m/z = 203.0549). Then $C_8H_{10}O_6$ degrades to form alkoxy radical and results in the formation of $C_4H_6O_2$ (m/z = 87.0454) and $C_4H_4O_2$ (m/z = 85.0289). $O_2^{\cdot-}$ may have a nucleophilic addition on carbonyl group (pathway C) and react with itself to form another tetroxide, and the corresponding aldehyde or carboxylic acid $C_4H_6O_2$ (m/z = 87.0447) is generated through a similar approach as above.

The formation of higher molecular weight compounds is observed, and the pathway of $^{\cdot}OH$ and $O_2^{\cdot-}$ to oxidize MACR is different. The photooxidation of MACR in the Fe(III)-Ox system is an important source of SOA in the atmosphere.

Small organic acids are known to be the main oxidation products of MACR (El Haddad et al., 2009). So, IC was used to analyze the 60 min photooxidation sample of MACR in Fe(III)-Ox and H_2O_2 systems. Photolysis of H_2O_2 only produces $^{\cdot}OH$, and the product is compared with the oxidation product from the Fe(III)-Ox system. Similar MACR photooxidation rates are obtained in 200 mM H_2O_2 after 60 min compared with the Fe(III)-Ox system. The results of IC measurements are shown in Fig. 9. Except for the oxalate added at the beginning, acetic, formic and pyruvic acids are detected in photolysis of MACR in the Fe(III)-Ox system, although pyruvic acid is not detected in the H_2O_2 system. The concentrations of small organic acids in the two systems have obvious differences. More acetic acid and less formic acid are obtained from the Fe(III)-Ox system. This may be because the oxidation mechanism of MACR in the two systems differs, and the involvement of $O_2^{\cdot-}$ influences the concentration of the products dramatically.

As shown in Fig. 10, the absorbance of the solution changes significantly with irradiation time. Two big absorbance peaks are found at around 280 nm and 310 nm at the beginning of the reaction, which from oxalate and MACR, respectively. The absorbance at 310 nm decreases in the first 30 min, and the absorbance of 280 nm relative to the nearby baseline decreases in the first 10 min, increases from 10 min to 60 min, then decreases from 60 min to 180 min. The absorbance of the region with a wavelength higher than 320 nm increases from 30 min to 150 min. The increasing absorbance at 280 nm might be due to the $n \rightarrow \pi^*$ transition of the intermediate products, such as aldehyde or ketone. The increasing absorbance of other parts comes from the formation of yellow precipitates $Fe(OH)_n$, which absorb light in the short wavelength, not from the oxidation products of MACR (Fig. A6). The clear yellow precipitates are produced in the late stage of the reaction. This finding indicates that the absorbance change caused by Fenton reaction might be an ignored factor, which would change the optical properties of aerosols and has implications for radiative forcing (Pillar-Little and Guzman, 2018).

4. Conclusions

The photooxidation mechanism of MACR with Fe(III)-Ox in atmospheric water was studied through bulk experiments. MACR was barely directly photolyzed under simulated sunlight (>290 nm) irradiation, and it had little oxidation when Fe(III) was involved. A large amount of MACR was oxidized by $^{\cdot}OH$ and $O_2^{\cdot-}$ when Fe(III) and oxalate existed together under simulated sunlight irradiation conditions. This finding indicated that the presence of Fe(III) and oxalate greatly enhanced the oxidation ability in atmospheric water through the consumption of oxalate in Fe(III)-Ox.

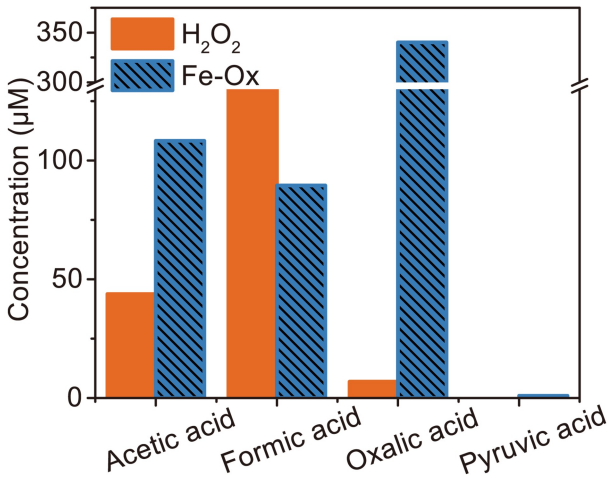

Fig. 9. Concentration of small organic acids in the photooxidation of MACR in H_2O_2 and Fe(III)-Ox system at 60 min obtained by IC ($[Fe(III)]_0$ = 100 μM, $[Oxalate]_0$ = 1000 μM, $[MACR]_0$ = 500 μM, pH 4.0 ± 0.1).

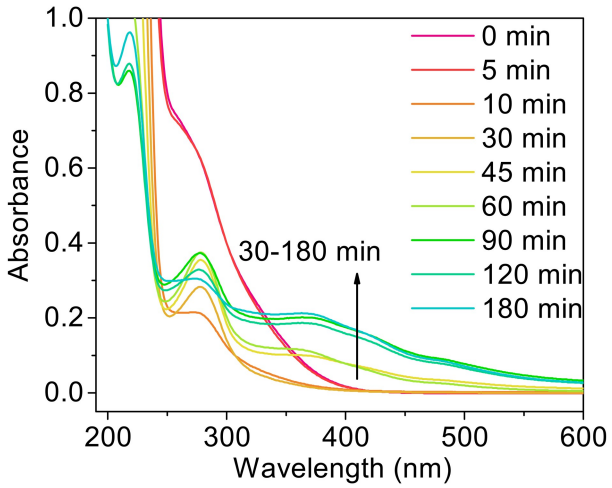

Fig. 10. The UV-Vis spectra of the photooxidation of MACR in Fe(III)-Ox system after filtering with 0.22 μm filter ($[Fe(III)]_0$ = 100 μM, $[Oxalate]_0$ = 1000 μM, $[MACR]_0$ = 500 μM, pH 4.0 ± 0.1, air-saturated solution).

The recycling of Fe(II) and Fe(III) led to the generation of H_2O_2 and ·OH, which contributed to the oxidation capacity. The increase of pH during the reaction caused the production of $Fe(OH)_n$ precipitate, which hindered the circulation of Fe(III) and Fe(II); it also caused the increase of the solution absorbance, which further affected the absorbance of aerosols and radiative forcing. The reaction pathways of the photooxidation of MACR in the Fe(III)-Ox system involving ·OH and $O_2^{\cdot-}$ were proposed. The photooxidation of MACR in the Fe(III)-Ox system could produce a different concentration of small organic acids compared to the photolysis H_2O_2 system, which only contained ·OH. This further shows that $O_2^{\cdot-}$ plays an important role in the oxidation of MACR. Additionally, oligomers with higher molecular weight were also observed in LC-QTOF-MS, and this finding indicates that MACR oxidation in the Fe(III)-Ox system could lead to SOA formation.

Acknowledgements. The authors gratefully acknowledge financial support from the Ministry of Science and Technology of the People's Republic of China (Grant Nos. 2017YFC0210005 and 2016YFE0112200).

APPENDIX

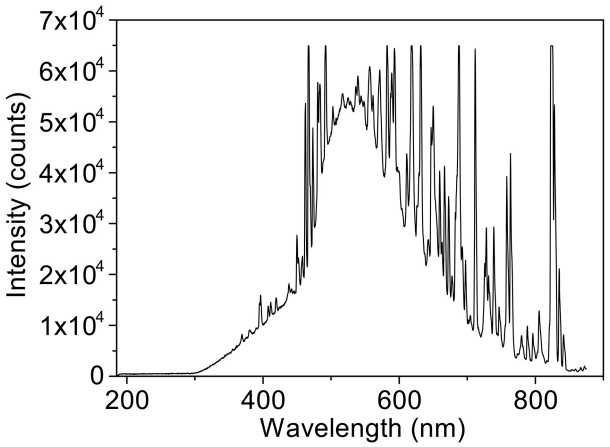

Fig. A1. The xenon lamp spectrum received by the reaction solution.

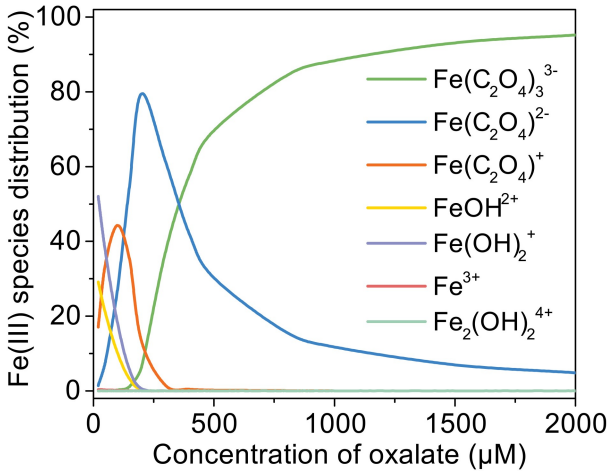

Fig. A3. Change of Fe(III) species distribution with oxalate concentration, $[Fe(III)]_0$ = 100 μM, pH = 4.0, 25°C.

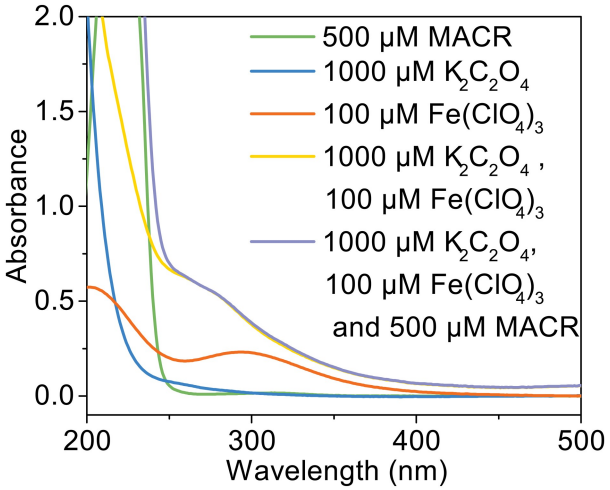

Fig. A2. UV-vis absorption spectra of solution (pH = 4.0 ± 0.1, in dark condition).

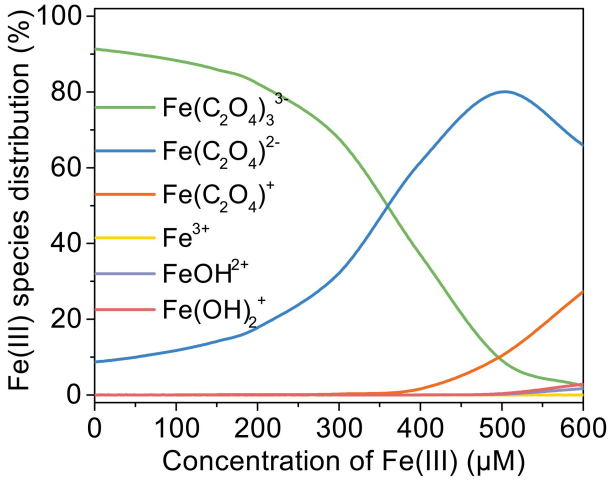

Fig. A4. Change of Fe(III) species distribution with Fe(III) concentration, $[Oxalate]_0$ = 1000 μM, pH = 4.0, 25°C.

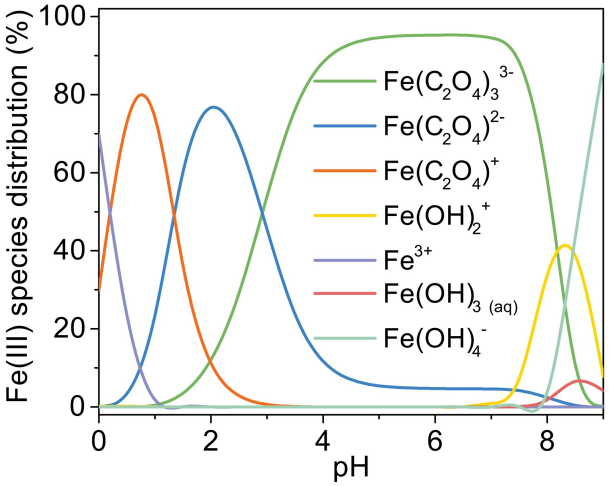

Fig. A5. Change of Fe(III) species distribution with pH, $[Fe(III)]_0$ = 100 μM, $[Oxalate]_0$ = 1000 μM, 25°C.

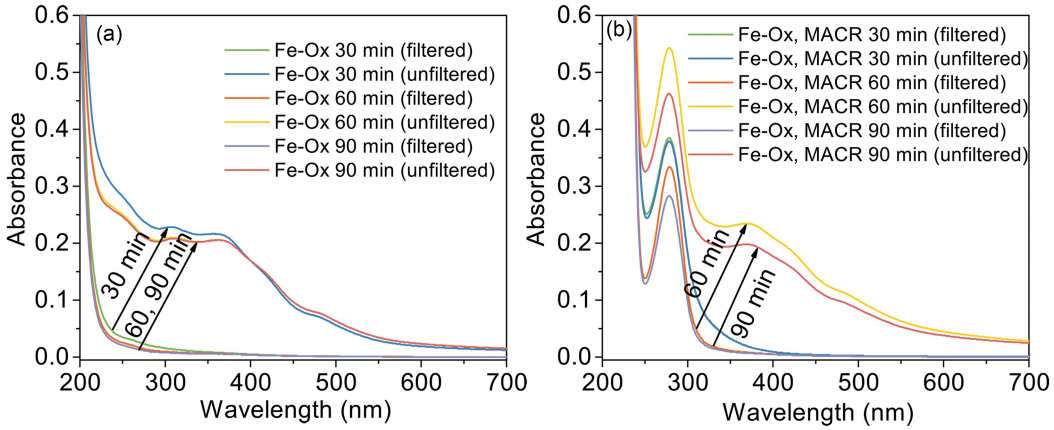

Fig. A6. The UV-Vis spectra of filtered (0.22 μm) and unfiltered (a) photolysis of the Fe(III)-Ox system, and (b) the photooxidation of MACR in the Fe(III)-Ox system ($[Fe(III)]_0$ = 100 μM, $[Oxalate]_0$ = 1000 μM, $[MACR]_0$ = 500 μM, pH 4.0 ± 0.1, air-saturated solution).

REFERENCES

Balmer, M. E., and B. Sulzberger, 1999: Atrazine degradation in irradiated iron/oxalate systems: Effects of pH and oxalate. *Environmental Science & Technology*, **33**, 2418–2424, https://doi.org/10.1021/es9808705.

Boreddy, S. K. R., K. Kawamura, and E. Tachibana, 2017: Long-term (2001–2013) observations of water-soluble dicarboxylic acids and related compounds over the western North Pacific: Trends, seasonality and source apportionment. *Scientific Reports*, **7**, 8518, https://doi.org/10.1038/s41598-017-08745-w.

Chu, B. W., and Coauthors, 2014: Decreasing effect and mechanism of $FeSO_4$ seed particles on secondary organic aerosol in α-pinene photooxidation. *Environmental Pollution*, **193**, 88–93, https://doi.org/10.1016/j.envpol.2014.06.018.

de Lima Perini, J. A., M. Perez-Moya, and R. F. P. Nogueira, 2013: Photo-Fenton degradation kinetics of low ciprofloxacin concentration using different iron sources and pH. *Journal of Photochemistry and Photobiology A: Chemistry*, **259**, 53–58, https://doi.org/10.1016/j.jphotochem.2013.03.002.

de Luca, A., R. F. Dantas, and S. Esplugas, 2014: Assessment of iron chelates efficiency for photo-Fenton at neutral pH. *Water Research*, **61**, 232–242, https://doi.org/10.1016/j.watres.2014.05.033.

Deguillaume, L., M. Leriche, A. Monod, and N. Chaumerliac, 2004: The role of transition metal ions on HOx radicals in clouds: A numerical evaluation of its impact on multiphase chemistry. *Atmospheric Chemistry and Physics*, **4**, 95–110, https://doi.org/10.5194/acp-4-95-2004.

Deguillaume, L., M. Leriche, and N. Chaumerliac, 2005: Impact of radical versus non-radical pathway in the Fenton chemistry on the iron redox cycle in clouds. *Chemosphere*, **60**, 718–724, https://doi.org/10.1016/j.chemosphere.2005.03.052.

El Haddad, I., and Coauthors, 2009: In-cloud processes of methacrolein under simulated conditions–Part 2: Formation of secondary organic aerosol. *Atmospheric Chemistry and Physics*, **9**, 5107–5117, https://doi.org/10.5194/acp-9-5107-2009.

Faust, B. C., and J. Hoigné, 1990: Photolysis of Fe (III)-hydroxy complexes as sources of OH radicals in clouds, fog and rain. *Atmos. Environ.*, **24**, 79–89, https://doi.org/10.1016/0960-1686(90)90443-Q.

Faust, B. C., R. G. Zepp, and Technology, 1993: Photochemistry of aqueous iron(III)-polycarboxylate complexes: Roles in the chemistry of atmospheric and surface waters. *Environmental Science & Technology*, **27**, 2517–2522, https://doi.org/10.1021/es00048a032.

Giorio, C., and Coauthors, 2017: Cloud processing of secondary organic aerosol from isoprene and methacrolein photooxidation. *The Journal of Physical Chemistry A*, **121**, 7641–7654, https://doi.org/10.1021/acs.jpca.7b05933.

Guasco, T. L., and Coauthors, 2014: Transition metal associations with primary biological particles in sea spray aerosol generated in a wave channel. *Environmental Science & Technology*, **48**, 1324–1333, https://doi.org/10.1021/es403203d.

Hayyan, M., M. A. Hashim, and I. M. AlNashef, 2016: Superoxide ion: Generation and chemical implications. *Chemical Reviews*, **116**, 3029–3085, https://doi.org/10.1021/acs.chemrev.5b00407.

Herrmann, H., T. Schaefer, A. Tilgner, S. A. Styler, C. Weller, M. Teich, and T. Otto, 2015: Tropospheric aqueous-phase chemistry: Kinetics, mechanisms, and its coupling to a changing gas phase. *Chemical Reviews*, **115**, 4259–4334, https://doi.org/10.1021/cr500447k.

Knight, R. J., and R. N. Sylva, 1975: Spectrophotometric investigation of iron(III) hydrolysis in light and heavy water at 25°C. *Journal of Inorganic and Nuclear Chemistry*, **37**, 779–783, https://doi.org/10.1016/0022-1902(75)80539-2.

Lazrus, A. L., G. L. Kok, S. N. Gitlin, J. A. Lind, and S. E. McLaren, 1985: Automated fluorimetric method for hydrogen peroxide in atmospheric precipitation. *Analytical Chemistry*, **57**, 917–922, https://doi.org/10.1021/ac00281a031.

Legrand, M., S. Preunkert, T. Oliveira, C. A. Pio, S. Hammer, A. Gelencsér, A. Kasper-Giebl, and P. Laj, 2007: Origin of C_2–C_5 dicarboxylic acids in the European atmosphere inferred from year-round aerosol study conducted at a west-east transect. *J. Geophys. Res.*, **112**, D23S07, https://doi.org/10.1029/2006JD008019.

Li, W. J., and Coauthors, 2016: A review of single aerosol particle studies in the atmosphere of East Asia: Morphology, mixing state, source, and heterogeneous reactions. *Journal of Cleaner Production*, **112**, 1330–1349, https://doi.org/10.1016/j.jclepro.2015.04.050.

Lian, L. S., S. W. Yan, B. Yao, S. A. Chan, and W. H. Song, 2017: Photochemical transformation of nicotine in wastewater effluent. *Environmental Science & Technology*, **51**, 11 718–11 730, https://doi.org/10.1021/acs.est.7b03223.

Liati, A., D. Schreiber, P. Dimopoulos Eggenschwiler, and Y. Arroyo Rojas Dasilva, 2013: Metal particle emissions in the exhaust stream of diesel engines: An electron microscope study. *Environmental Science & Technology*, **47**, 14 495–14 501, https://doi.org/10.1021/es403121y.

Liu, Y., and Coauthors, 2009: In-cloud processes of methacrolein under simulated conditions–Part 1: Aqueous phase photooxidation. *Atmospheric Chemistry and Physics*, **9**, 5093–5105, https://doi.org/10.5194/acp-9-5093-2009.

Liu, Y., and Coauthors, 2012: Oligomer and SOA formation through aqueous phase photooxidation of methacrolein and methyl vinyl ketone. *Atmos. Environ.*, **49**, 123–129, https://doi.org/10.1016/j.atmosenv.2011.12.012.

Mulazzani, Q. G., M. D'Angelantonio, M. Venturi, M. Z. Hoffman, and M. A. J. Rodgers, 1986: Interaction of formate and oxalate ions with radiation-generated radicals in aqueous solution. Methylviologen as a mechanistic probe. *The Journal of Physical Chemistry*, **90**, 5347–5352, https://doi.org/10.1021/j100412a090.

Nguyen, T. B., M. M. Coggon, R. C. Flagan, and J. H. Seinfeld, 2013: Reactive uptake and photo-Fenton oxidation of glycolaldehyde in aerosol liquid water. *Environmental Science & Technology*, **47**, 4307–4316, https://doi.org/10.1021/es400538j.

Pang, H. W., and Coauthors, 2019: Photochemical aging of guaiacol by Fe(III)-oxalate complexes in atmospheric aqueous phase. *Environmental Science & Technology*, **53**, 127–136, https://doi.org/10.1021/acs.est.8b04507.

Patel, K. B., and R. L. Willson, 1973: Semiquinone free radicals and oxygen. Pulse radiolysis study of one electron transfer equilibria. *Journal of the Chemical Society, Faraday Transactions 1: Physical Chemistry in Condensed Phases*, **69**, 814–825, https://doi.org/10.1039/F19736900814.

Pillar-Little, E. A., and M. I. Guzman, 2018: An overview of dynamic heterogeneous oxidations in the troposphere. *Environments*, **5**, 104, https://doi.org/10.3390/environments5090104.

Rush, J. D., and B. H. J. Bielski, 1985: Pulse radiolytic studies of the reactions of HO_2/O_2^- with Fe (II)/Fe (III) ions. The reactivity of HO_2/O_2^- with ferric ions and its implication on the occurrence of the Haber-Weiss reaction. *J. Phys. Chem.*, **89**, 5062–5066, https://doi.org/10.1021/j100269a035.

Sastry, C. S. P., and J. S. V. M. L. Rao, 1996: Determination of doxorubicin hydrochloride by visible spectrophotometry. *Talanta*, **43**, 1827–1835, https://doi.org/10.1016/0039-9140(96)01932-7.

Schöne, L., J. Schindelka, E. Szeremeta, T. Schaefer, D. Hoffmann, K. J. Rudzinski, R. Szmigielski, and H. Herrmann, 2014: Atmospheric aqueous phase radical chemistry of the isoprene oxidation products methacrolein, methyl vinyl ketone, methacrylic acid and acrylic acid-kinetics and product studies. *Physical Chemistry Chemical Physics*, **16**, 6257–6272, https://doi.org/10.1039/C3CP54859G.

Sedlak, D. L., and J. Hoigné, 1993: The role of copper and oxalate in the redox cycling of iron in atmospheric waters. *Atmospheric Environment. Part A. General Topics*, **27**, 2173–2185, https://doi.org/10.1016/0960-1686(93)90047-3.

Seinfeld, J. H., and S. N. Pandis, 2016: *Atmospheric Chemistry and Physics: From Air Pollution to Climate Change*. 3rd ed. Wiley.

Sorooshian, A., and Coauthors, 2006: Oxalic acid in clear and cloudy atmospheres: Analysis of data from international consortium for atmospheric research on transport and transformation 2004. *J. Geophys. Res.*, **111**, D23S45, https://doi.org/10.1029/2005JD006880.

Sorooshian, A., Z. Wang, M. M. Coggon, H. H. Jonsson, and B. Ervens, 2013: Observations of sharp oxalate reductions in stratocumulus clouds at variable altitudes: Organic acid and metal measurements during the 2011 E-PEACE campaign. *Environmental Science & Technology*, **47**, 7747–7756, https://doi.org/10.1021/es4012383.

Surdhar, P. S., S. P. Mezyk, and D. A. Armstrong, 1989: Reduction potential of the carboxyl radical anion in aqueous solutions. *The Journal of Physical Chemistry*, **93**, 3360–3363, https://doi.org/10.1021/j100345a094.

Thomas, D. A., and Coauthors, 2016: Real-time studies of iron oxalate-mediated oxidation of glycolaldehyde as a model for photochemical aging of aqueous tropospheric aerosols. *Environmental Science & Technology*, **50**, 12 241–12 249,

https://doi.org/10.1021/acs.est.6b03588.

van Pinxteren, D., and Coauthors, 2005: Schmücke hill cap cloud and valley stations aerosol characterisation during FEBUKO (II): Organic compounds. *Atmosp. Environ.*, **39**, 4305–4320, https://doi.org/10.1016/j.atmosenv.2005.02.014.

Weller, C., S. Horn, and H. Herrmann, 2013a: Photolysis of Fe(III) carboxylato complexes: Fe(II) quantum yields and reaction mechanisms. *Journal of Photochemistry and Photobiology A: Chemistry*, **268**, 24–36, https://doi.org/10.1016/j.jphotochem.2013.06.022.

Weller, C., S. Horn, and H. Herrmann, 2013b: Effects of Fe(III)-concentration, speciation, excitation-wavelength and light intensity on the quantum yield of iron(III)-oxalato complex photolysis. *Journal of Photochemistry and Photobiology A: Chemistry*, **255**, 41–49, https://doi.org/10.1016/j.jphotochem.2013.01.014.

Weller, C., A. Tilgner, P. Bräuer, and H. Herrmann, 2014: Modeling the impact of iron-carboxylate photochemistry on radical budget and carboxylate degradation in cloud droplets and particles. *Environmental Science & Technology*, **48**, 5652–5659, https://doi.org/10.1021/es4056643.

Zhang, X., Z. M. Chen, and Y. Zhao, 2010: Laboratory simulation for the aqueous OH-oxidation of methyl vinyl ketone and methacrolein: Significance to the in-cloud SOA production. *Atmospheric Chemistry and Physics*, **10**, 9551–9561, https://doi.org/10.5194/acp-10-9551-2010.

Zhou, S. Q., J. Lin, X. F. Qin, Y. Chen, and C. R. Dneg, 2018: Determination of atmospheric alkylamines by ion chromatography using 18-crown-6 as mobile phase additive. *Journal of Chromatography A*, **1563**, 154–161, https://doi.org/10.1016/j.chroma.2018.05.074.

Zuo, Y. G., and J. Hoigne, 1992: Formation of hydrogen peroxide and depletion of oxalic acid in atmospheric water by photolysis of iron(III)-oxalato complexes. *Environmental Science & Technology*, **26**, 1014–1022, https://doi.org/10.1021/es00029a022.